JOURNAL OF AIRCRAFT
Vol. 29, No. 6, Nov.–Dec. 1992

Transonic Low-Reynolds Number Airfoils

Mark Drela*
Massachusetts Institute of Technology, Cambridge, Massachusetts 02139

Airfoils operating in the unexplored high-Mach—low-Reynolds number regime are computationally investigated. The motivations are 1) quantification of achievable airfoil performance levels; 2) quantification of parameter sensitivities which impact vehicle sizing; 3) identification of possible shortcomings in the computational methods employed; and 4) identification of test data required for adequate validation of the airfoil designs and performance prediction methods. The investigation centers on candidate airfoils developed for proposed ultrahigh altitude aircraft (UHAA) having both a high-ceiling and a long-range requirement. Computational studies indicate that 35-km ceiling performance at $M \simeq 0.60$, $Re \simeq 200{,}000$ hinges on the effective use of transonic flow to enhance transition and reduce separation-bubble losses. The separation bubbles become associated with large lambda shock structures at the highest tolerable Mach numbers. Airfoil performance predictions are parameterized by quantities dependent only on altitude and vehicle characteristics, and independent of flight trim conditions. For the airfoils designed, no flaps are necessary to achieve nearly optimal performance at both 35-km ceiling conditions as well as lower 15–25-km altitudes where long-range cruise would occur. Variation in airfoil thickness between 11–15% has surprisingly little impact on aerodynamic performance.

Nomenclature

AR	=	wing aspect ratio
a	=	freestream speed of sound
C_D	=	profile drag coefficient
C_L	=	profile lift coefficient
C_p	=	pressure coefficient
c	=	average wing chord
H	=	boundary-layer shape parameter, δ^*/θ
M, M_∞	=	freestream Mach number, V/a
M_e	=	boundary-layer edge Mach number
$\mathcal{M}$	=	reduced Mach number, $M\sqrt{C_L}$
n_{crit}	=	critical amplification ratio
p	=	freestream pressure
$\mathcal{R}$	=	reduced Reynolds number, $Re\sqrt{C_L}$
Re	=	chord Reynolds number, $\rho Vc/\mu$
S	=	wing area
u_e	=	boundary-layer edge velocity
V	=	freestream speed
W	=	vehicle weight
α	=	angle of attack
γ	=	ratio of specific heats
δ^*	=	boundary-layer displacement thickness
θ	=	boundary-layer momentum thickness
μ	=	freestream viscosity
ρ	=	freestream density

I. Introduction

CURRENT interest in ultrahigh altitude aircraft (UHAA) stems from their potential value in conducting atmospheric science research. The severe cost and performance limitations of current ER-2 and balloon platforms could be largely overcome with the advanced UHAA platforms, such as the *HAARP* proposed by NASA,[1] and the *Theseus* proposed by Aurora Flight Sciences.[2] Altitudes of up to 35 km are being targeted by these new designs, largely made possible by modern composite structural technology and high-specific energy propulsion systems. In contrast, the excessive wing loading of the all-aluminum ER-2 limits it to a 23-km ceiling, while the experimental Boeing *Condor*[3] aircraft has a reported 20-km ceiling apparently set by propulsion system limitations.

The 35-km ceiling targeted with the new UHAA platforms puts extraordinary demands on airfoil performance. Figure 1 shows the ceiling parameter M^2C_L which must be achieved by the aircraft as a function of altitude and wing loading. To reach an altitude of 35 km (115,000 ft), the *Theseus* aircraft must attain $C_L \simeq 1.30$ at Mach and Reynolds numbers of $M \simeq 0.6$ and $Re = 200{,}000$. This high-Mach—low-Reynolds number combination is quite unique in aeronautical applications, and is unfortunately distinguished by a complete lack of suitable airfoil data (see Fig. 2).

Subsonic low-Reynolds number airfoil design is now fairly well understood, the key issue being control of transitional separation bubbles by encouraging transition at the appropriate location. This can be achieved by means of appropriately tailored pressure distributions,[4,5] and/or by forcing transition by way of mechanical or pneumatic means.[6,7] Consideration has also been given to controlling bubble losses over an appropriate C_L range in the theoretical and experimental study of Selig et al.[8] Since transition mechanisms found on airfoils (e.g., Tollmien-Schlichting waves) are not qualitatively affected by higher Mach numbers, the same low-Reynolds number airfoil design strategies should be directly applicable to transonic speeds. The presence of transonic flow will, of course,

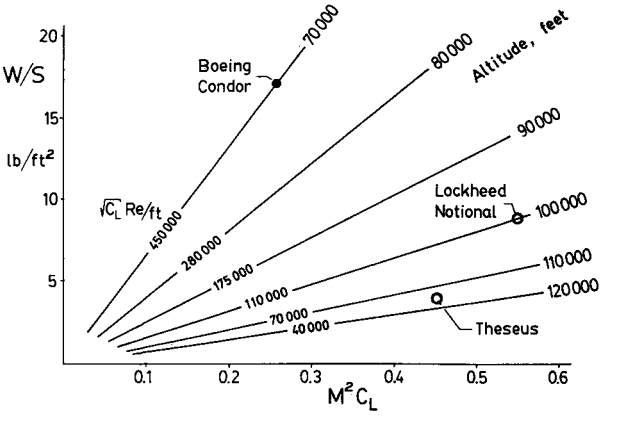

Fig. 1 Required ceiling parameter M^2C_L vs wing loading for various altitudes.

Received Feb. 28, 1991; revision received Aug. 27, 1991; presented as Paper 91-3337 at the AIAA 9th Applied Aerodynamics Conference, Baltimore, MD, Sept. 23–25, 1991; accepted for publication Dec. 21, 1991.

*T. Wilson Associate Professor, Department of Aeronautics and Astronautics. Member AIAA.

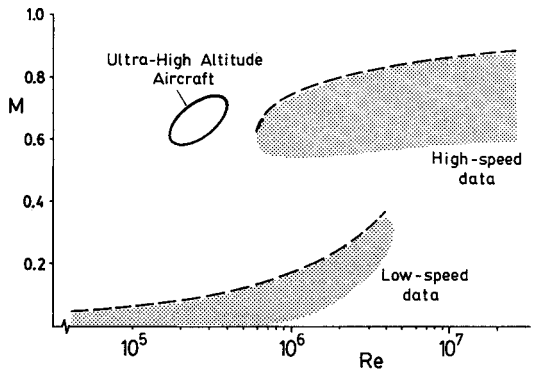

Fig. 2 Limits of available airfoil data.

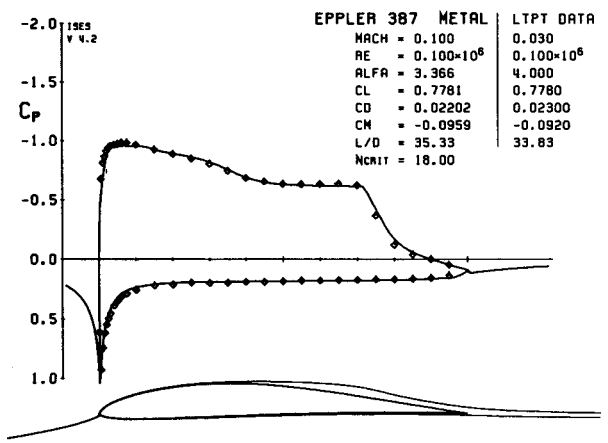

Fig. 3 Computed and experimental pressure distributions and force coefficients for the Eppler 387 airfoil.

influence the quantitative performance of the airfoils and their off-design behavior.

The present study relies extensively on the coupled viscous/inviscid ISES code.[9,10] It uses a conservative finite-volume streamline grid Euler formulation to represent the outer flow, and a two-equation dissipation integral formulation to represent the viscous layers. The two regions are coupled by way of the displacement thickness. The ISES code has been found to be very reliable for essentially all of the types of airfoil flows found in aeronautical applications, from high-Reynolds number transonic transport airfoils to low-Reynolds number low-speed airfoils. A recent modification has been to replace the separated branch of the Falkner-Skan laminar closure correlations with correlations derived from nonsimilar profiles generated with a finite-difference boundary-layer code. Such nonsimilar profiles are more representative of those found in typical separation bubbles, and therefore, give better predictions of bubble-dominated flows. Figure 3 compares a computed solution with the high-quality low-Mach number data of McGhee et al.[11]

Liebeck[12] has recently used the ISES code in a computational study of high-lift airfoils at Reynolds numbers between $\frac{1}{2}$–2 million and Mach numbers up to 0.5. The separation bubble invariably present on subcritical low-Reynolds number airfoils was found to be associated with a λ-shock once supercritical flow was attained at higher Mach numbers. Similar computational examples will be given in the next section. The presence of the λ-shock is significant in that it alters the response of the outer flow pressure to displacement surface perturbations. This response is what essentially controls the bubble height (or shape parameter) distribution over the bubble, which in turn affects instability growth rates and transition location.[5] The location of the transition point and the bubble losses will therefore have a different dependence on C_L, e.g., than in subcritical flow. Supersonic outer flow at the bubble also raises a number of questions concerning modeling of upstream influence in the boundary layer, and the accuracy of the ISES integral boundary layer and transition models for this situation.

The present paper will examine the issues discussed above in the context of airfoils designed for the proposed *HAARP* and/or *Theseus* aircraft. The primary goal is to identify the limits to airfoil performance in the unexplored high-Mach—low-Reynolds number regime. Sensitivities to operating parameters and airfoil thickness will also be investigated, since such information is vital to mission development and initial sizing of a prospective UHAA. A related goal is to identify those aspects of the ISES calculation method which are critical to accurate performance predictions. Potential targets for any future experimental and theoretical work will also be identified.

II. Transonic Flow Effects

The interaction of supercritical flow with a transitional separation bubble is illustrated using the above-mentioned Eppler 387 low-Reynolds number airfoil as an example. Figure 4 shows the predicted subcritical $M_\infty = 0.60$) and supercritical ($M_\infty = 0.65$) C_p distributions for this airfoil at a chord Reynolds number of 200,000. The calculations were performed using the ISES code. Although the C_p distributions over the

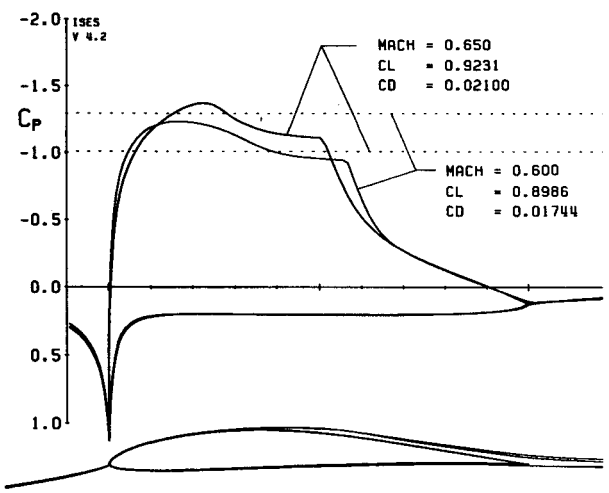

Fig. 4 Predicted C_p vs x/c on Eppler 387 for subcritical and supercritical flow at $\alpha = 3$ deg, $Re = 200{,}000$.

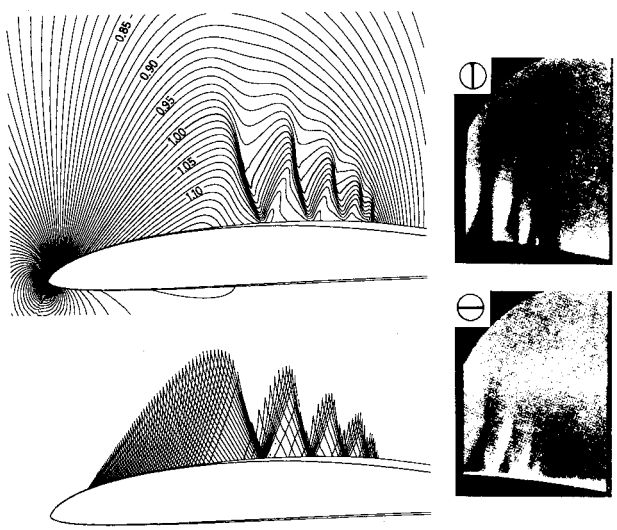

Fig. 5 Mach contours and Mach lines for Eppler 387 airfoil at $M_\infty = 0.65$, $Re = 200{,}000$, and $\alpha = 3$ deg, showing λ-shocks over separation bubble. Schlieren photograph shows shocks on generic tunnel model.

separation bubbles are qualitatively similar, the bubble in the supercritical case is associated with a λ-shock, which is clearly visible in the dense Mach contour plot in Fig. 5. Also shown are the Mach lines, which reveal the supersonic wave structure. For qualitative comparison, Fig. 5 also shows a schlieren photo from Ackeret et al.[14] with multiple λ-shocks over a generic tunnel model. The peak Mach numbers in the experiment ($M_{max} = 1.141$) and the calculation ($M_{max} = 1.160$) are nearly the same, and the flowfields compare quite well.

The early experimental and theoretical investigation of Liepmann[13] and Ackeret et al.[14] identified the relevant features of λ-shock flows. A precompression wave separates the laminar boundary layer well ahead of the first shock, which impinges on the separated free shear layer and reflects as an expansion wave. The expansion may be followed by subsequent λ-shocks, the number of which depends on the Mach and Reynolds numbers.

An interesting feature of such a shock/boundary-layer interaction is that past the separation point, the shocks do not affect the surface pressure distribution, this being controlled entirely by the free shear layer. The steep pressure rise to subcritical conditions is apparently due to transition in the shear layer and not an impinging shock. An important question is whether or not the shocks reflecting off the separated free shear layer introduce significant initial Tollmien-Schlichting disturbances. No theoretical treatment of this problem has been attempted to the author's knowledge. Any effect on transition is significant in that it impacts the loss of the overall separation bubble and the airfoil drag. This issue of transition modeling for these flows will be discussed later.

III. Computational Modeling

The accuracy of the above numerical predictions hinges on the accuracy of the ISES outer flow solver, the accuracy of the boundary-layer formulation, and the validity of the displacement model used to couple the viscous and inviscid regions. An important feature of boundary-layer equations is that once past laminar separation, they can only admit nearly zero pressure gradient and little or no constraint is imposed on the displacement thickness. The latter is set by the outer inviscid flow, which is free to position the displacement surface so that it is a constant-pressure streamline as required by the boundary-layer equations. If a shock impinges on the displacement surface, then it must be reflected as an expansion wave to maintain the zero streamwise pressure gradient. These are the essential features of the physical model proposed by Liepmann.[13] Normal pressure gradients, which in turbulent interactions often cast the boundary-layer approximations into doubt,[15] cannot be transmitted into the stagnant fluid under the free shear layer. The lack of this normal pressure gradient, plus the simple free shear-layer interaction mechanism, make it very likely that an inviscid solver coupled to the standard boundary-layer equations is fully adequate for λ-shock interactions.

To gain confidence in this computational model for λ-shocks, calculations were performed for the 12% thick double-circular arc airfoil used in the tests reported in Ref. 13. Unfortunately, the test airfoil model had an aspect ratio of only 0.667, resulting in large sidewall influence on the transonic flow. The test section sidewalls were diverged slightly to allow for the growth of the sidewall boundary layers, so that a uniform streamwise pressure was obtained in the empty tunnel. Except in the immediate vicinity of the leading and trailing edges, the lowered pressure caused by the acceleration over the airfoil would cause a thinning of the sidewall boundary layers ahead of the airfoil midchord, and a thickening behind it. This would produce an effectively wider channel at the model itself. The effect can be estimated from the von Karman integral momentum equation, which relates changes in velocity and momentum thickness as follows:

$$\frac{\Delta\theta}{\theta} \simeq -(H + 2 - M_e^2)\frac{\Delta u_e}{u_e} \qquad (1)$$

Taking $H = 1.5$, $M_e^2 = 1.0$, and a typical velocity change $\Delta u_e/u_e = 0.2$ (from $M \simeq 0.8$ to $M \simeq 1.0$), and assuming that the shape parameter remains roughly constant, gives

$$\frac{\Delta\delta^*}{\delta^*} = \frac{\Delta\theta}{\theta} \simeq -0.5 \qquad (2)$$

To cancel the sidewall boundary-layer growth, the tunnel width was reportedly increased by 10% over the length of the test section. This implies that at the model near the center of the test section the total sidewall boundary-layer displacement thickness was about 5% of the channel width. Therefore, the effective channel width due to sidewall boundary-layer thinning near the model would increase by about $0.5 \times 5\% = 2.5\%$. For the $M_\infty \simeq 0.8$ freestream Mach numbers used in the tests, this tunnel width increase corresponds to a decrease of about

$$\Delta M_\infty \simeq -0.05 \qquad (3)$$

in the effective freestream Mach number seen by the airfoil.

Figure 6 shows the calculated surface Mach number distribution compared with experimental data taken at $M_\infty = 0.795$ and $Re = 833{,}000$. The calculation required a specified freestream Mach number of $M_\infty = 0.765$ in order to match the observed local peak Mach number on the model. This decrease of $\Delta M_\infty = -0.03$ reasonably matches the sidewall boundary-layer thinning effect estimated above. A critical amplification ratio of $n_{crit} = 12$ was specified for this calculation, which is appropriate for the reportedly high-tunnel flow quality. Although the peak Mach number at the airfoil midchord just barely exceeds unity, the flow is subcritical over the bubble pressure plateau, which has been captured reasonably well in the calculation. Significant differences are present between the measured and computed pressure gradients towards the leading and trailing edges, although these are in accordance with the sidewall boundary-layer thinning effect. The steep pressure rise (after transition in particular) would produce a strong response in the sidewall boundary layer to reduce the pressure gradient. This is supported by the fact that each sidewall boundary layer at the model is about six times thicker than the airfoil surface boundary layer just past the bubble, and will produce a proportionately greater displacement response.

Figure 7 shows the same circular arc airfoil at a higher freestream Mach number. The calculation required $M_\infty = 0.797$ in lieu of the experimental $M_\infty = 0.843$—a reasonable decrease of $\Delta M_\infty = -0.045$. Again, the bubble pressure plateau has been captured reasonably well, and the pressure gradients are again underpredicted. The flow over the bubble is supercritical in this case, giving the characteristic λ-shock

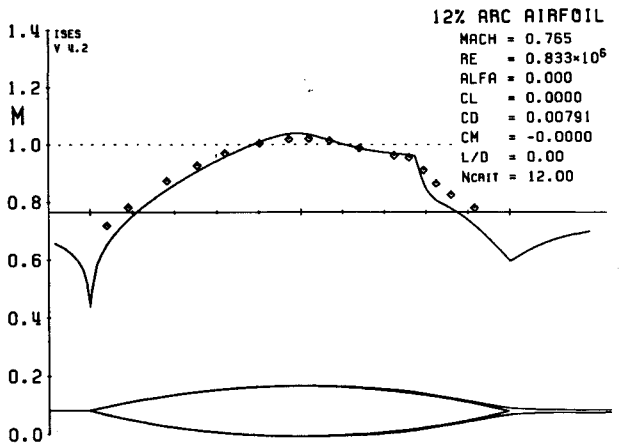

Fig. 6 Calculated and experimental Mach number distributions over a 12% thick circular arc airfoil. $Re = 833{,}000$, $M_\infty = 0.795$ (experimental), and $M_\infty = 0.765$ (computation).

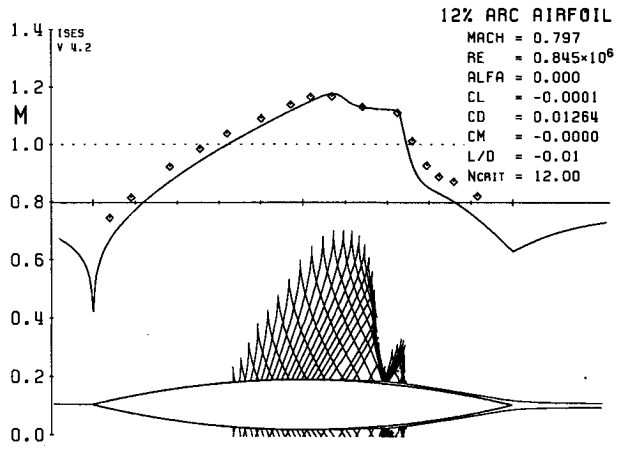

Fig. 7 Calculated and experimental Mach number distributions over 12% thick circular arc airfoil. Mach lines reveal double λ-shock. Re = 845,000, M_∞ = 0.843 (experimental), and M_∞ = 0.797 (computation).

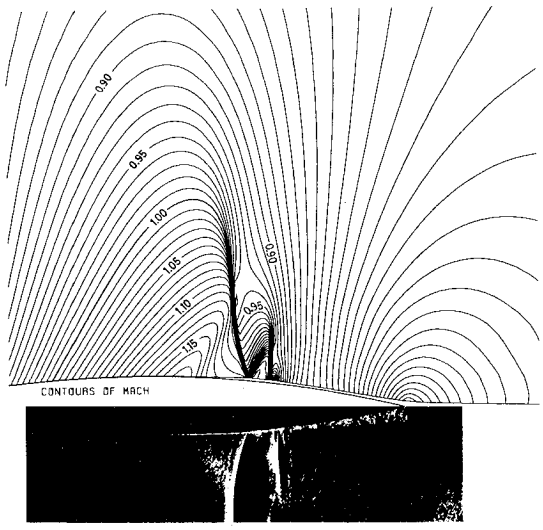

Fig. 8 Calculated Mach number contours for 12% thick circular arc airfoil, compared with experimental schlieren photograph. Re = 845,000, M_∞ = 0.843 (experimental), and M_∞ = 0.797 (computation).

revealed by the Mach lines displayed in Fig. 7. Figure 8 compares computed Mach number contours with a schlieren photo from the experiment. A 264 × 62 grid (twice the standard resolution) was used to better reveal the flow features, although the surface pressures are unaffected to within plotting accuracy. All the important features of the λ-shock structure have been captured extremely well in the calculation, including the smaller secondary shock.

The above comparisons with experimental data, at the very least, give confidence that the viscous/inviscid methodology of the ISES code adequately models all the flow physics required to capture λ-shocks. Since the data is clearly contaminated by sidewall effects, questions concerning the quantitative accuracy of the predictions still remain. A better evaluation would require high-quality two-dimensional data not currently available in the Mach and Reynolds number ranges of interest. In any case, the method appears to be adequate for the present goal of parameterically investigating low-Reynolds number transonic airfoil behavior.

Before proceeding to the airfoil design study, a few observations and comments are in order. It is interesting to note that the λ-shock interaction can be captured without a "correct" representation of the upstream pressure signal propagation in the subsonic portion of the laminar boundary layer. As is well known, it is this signal propagation in the physical situation which induces the boundary layer to separate well before the first shock. No such propagation is possible in the integral boundary-layer formulation, although the coupled viscous/inviscid scheme does contain a purely numerical upstream influence. Each boundary-layer station is located midway between two locations in the inviscid grid where the edge velocity is defined. These two velocities are averaged before being transferred to the boundary-layer point, thereby producing the upstream influence.

The final uncertainty in the overall computational model is the prediction of the transition location which sets the length of the bubble. The most important parameters influencing transition in separation bubbles are the Reynolds number and the ambient disturbance level. In the compressible case, the Mach number plays a lesser, although significant, role. The present transition formulation is essentially the e^n envelope method of Smith and Gamberoni[16] and von Ingen.[17] The local growth rate of the most-amplified Tollmein-Schlichting frequency is correlated to the local momentum thickness Reynolds number and the kinematic shape parameter. The ambient disturbance level enters the formulation by way of the specified critical amplification ratio n_{crit} mentioned above. The disturbance growth rates are determined from solutions of the incompressible Orr-Sommerfeld equation. Although compressibility clearly has an impact on the growth rates,[18] this is not presently accounted for. In particular, higher Mach numbers result in reduced growth rates, which delays transition in separation bubbles and increases their losses. The multiple λ-shocks impinging on the free shear layer, on the other hand, may introduce substantial disturbances and therefore reduce the bubble losses. Given this latter uncertainty, it is felt that a simple incompressible stability formulation is adequate for parametrically investigating the solution sensitivity to background disturbance levels by systematic variation of the n_{crit} parameter.

IV. Airfoil Design Parameters

To minimize vehicle size and cost, and to maximize its robustness, it is desirable to use the highest wing loading compatible with the required mission. The exact relation

$$M^2 C_L = \frac{V^2}{a^2}\frac{2W}{\rho V^2 S} \tag{4}$$

$$= \frac{2}{\gamma}\frac{W/S}{p} \tag{5}$$

indicates that to maximize the wing loading W/S for a specified ceiling altitude (which fixes the ambient pressure p), the ceiling parameter $M^2 C_L$ must be made as large as possible. This parameter, which can be considered as the square of the "reduced" Mach number

$$\mathcal{M} \equiv M\sqrt{C_L} = \left(\frac{2}{\gamma}\frac{W/S}{p}\right)^{1/2} \tag{6}$$

is also significant in that it remains invariant as an aircraft undergoes trim (i.e., C_L) changes at a fixed altitude. Since this reduced Mach number $\mathcal{M}$ only depends on wing loading and the altitude, it is more natural for parameterizing airfoil characteristics than the usual Mach number M. Trim changes cause M to vary, which complicates the evaluation of airfoil behavior over a finite C_L range. Trim changes will also cause the Re to vary, and although this variation is normally negligible, at low-Reynolds numbers even small Reynolds number changes (percentage-wise) can have a large impact on the drag. Therefore, it is more appropriate to parameterize airfoil characteristics on the reduced Reynolds number $\mathcal{R}$

$$\mathcal{R} \equiv Re\sqrt{C_L} = \frac{\rho V c}{\mu}\left(\frac{2W}{\rho V^2 S}\right)^{1/2} \tag{7}$$

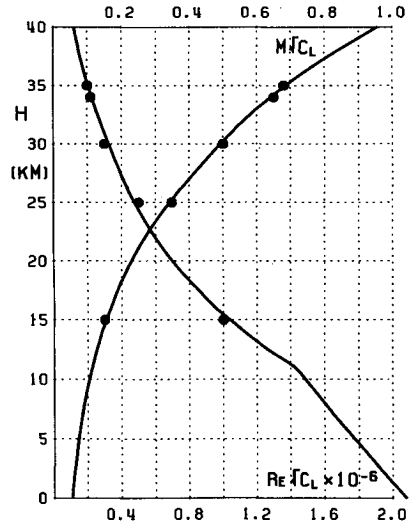

W/S = 200 N/m²
= 4.2 lb/ft²

S = 70 m²
= 750 ft²

AR = 25

Altitude	$\mathcal{M}$	$\mathcal{R}$
35 km	0.68	200 000
34 km	0.65	220 000
30 km	0.50	300 000
25 km	0.35	500 000
15 km	0.15	1 000 000

Fig. 9 Reduced Mach and Reynolds numbers vs altitude for representative ultrahigh altitude aircraft. Symbols are points examined.

$$= \left(\frac{2\rho}{\mu^2}\frac{W}{AR}\right)^{1/2} \tag{8}$$

as this also remains invariant with trim changes. Figure 9 shows the values of $\mathcal{M}$ and $\mathcal{R}$ which must be achieved as a function of altitude for a representative subsonic aircraft having a wing loading of W/S = 200 N/m², wing area of S = 70 m², and an aspect ratio of AR = 25, flying in a US standard atmosphere. These parameters, especially the rather low-wing loading, represent a practical limit with modern composite structural technology. For this particular wing loading, the rapid increase in reduced Mach number $\mathcal{M}$ and decrease in reduced Reynolds number $\mathcal{R}$ firmly limit the ceiling to about 35 km.

In the atmospheric sampling missions envisioned for a prospective aircraft, the 35-km altitude might be required for only some fraction of the data sampling runs. A significant amount of data aquisition would also occur at 30 km or perhaps at 25 km, depending on the type of mission. A large part of the flight time would also be spent flying to and from the sampling area. This might typically occur at 15 km, which is low enough to give conditions much more favorable to long range, but is still well above any weather. Figure 9 lists the parameter combinations encountered in this type of mission.

V. Airfoil Design Rationale

A. Airfoil Family

To allow systematic parameter studies, the TH12 airfoil was designed as a base airfoil from which variants would be derived. The TH12 is 12.9% thick and has substantial aft camber. Figure 10 shows the TH12 geometry together with two 14.9% and 10.9% thick variants, designated TH11 and TH13, respectively. The figure also compares their pressure distributions at a typical 35-km operating point. These differ considerably from the nearly flat "rooftop" suction surface pressure distribution found on a conventional high-Reynolds number supercritical airfoil. The low-Reynolds number design requirements which lead to the unconventional pressure distributions of the TH11–13 airfoils are discussed below.

B. Ceiling Conditions

Since the 35-km ceiling conditions are by far the most challenging, the airfoils were tailored for this point, and then modified for the lower altitude conditions as necessary. For a given reduced Mach number $\mathcal{M} = M\sqrt{C_L}$, it is desirable to employ the largest feasible C_L to reduce the Mach number M and the attendant drag to an absolute minimum. Low-Reynolds number airfoils tend to have their best C_L/C_D close

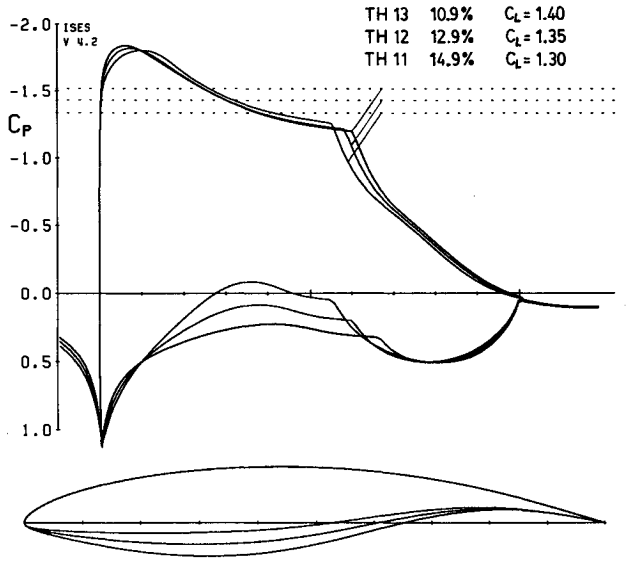

Fig. 10 Airfoils designed for transonic low-Reynolds number operation, with C_p distributions at $\mathcal{M}$ = 0.68 and $\mathcal{R}$ = 200,000 (at 35-km ceiling).

to stall, and this likewise dictates a large C_L. The final choice must of course reflect the Mach and Reynolds number variation with altitude.

Low-Reynolds number airfoil design centers on reducing the losses associated with transitional separation bubbles.[4] The lowest drag for any airfoil is typically obtained when transition occurs near the laminar separation point. For Reynolds numbers less than about 1 million, natural transition usually falls past this point, causing the separation bubble and increasing the drag. One approach to reducing the bubble size or eliminating it is to force transition earlier by pneumatic or mechanical means.[6,7] However, this approach may not be practical for the suction surface of airfoils which must operate over a large angle of attack and/or Reynolds number range,[5] as the optimum transition location will move drastically. For such applications an effective approach is to apply a long mild adverse pressure gradient to the laminar boundary layer ahead of and at the bubble wherever it may occur.[4] This triggers early instability growth and causes transition to occur acceptably soon after laminar separation. With the $M\sqrt{C_L}$ = 0.68 and high C_L requirements at 35 km, this can only be achieved with some supersonic flow near the leading edge, as shown in Fig. 10. After the initial supersonic expansion, a smooth recompression to subsonic flow achieves the desired adverse pressure gradient with no shock losses. A separation bubble is still formed, and although it is quite long, the maximum shape parameters incurred are reasonable and the bubble losses are not too detrimental. Keeping the bubble losses in check in this manner precludes relying on a flat rooftop pressure distribution characteristic of high-Reynolds number supercritical airfoils. Such airfoils would suffer bubble bursting and massive separation at low-Reynolds numbers.

The design pressure distributions shown in Fig. 10 have been compromised somewhat to attain a reasonably wide C_L range and adequate structural depth at the trailing edge. Lower bubble losses can be obtained with a longer and shallower adverse pressure gradient region started from very near the leading edge, and more load can be carried by undercutting the front lower surface.[7] However, both of these features have been found to substantially reduce the usable C_L range for only a very marginal design performance benefit. Likewise, increasing the aft lower camber gives marginal benefit, since new structural problems arise, and the increase in the lower boundary-layer displacement thickness mostly eliminates the added camber.

Although the pressure distributions shown in Fig. 10 are supercritical, the bubble pressure plateaus have been pur-

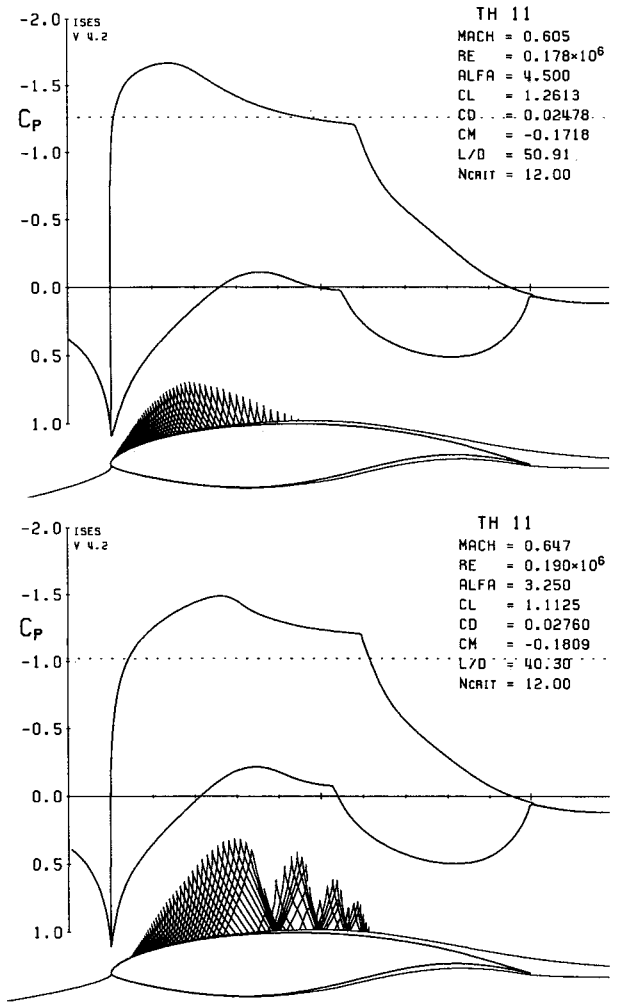

Fig. 11 C_p distributions for TH11 airfoil at 35-km operation at normal (C_L = 1.26) and overspeed (C_L = 1.11) conditions, $\mathcal{M}$ = 0.68 and $\mathcal{R}$ = 200,000.

posely kept subsonic to avoiding the formation of λ-shock structures. All calculations have indicated that these invariably lead to viscous drag increases (the momentum deficit of the shock itself is negligible) and therefore are undesirable in normal operation. The λ-shocks will appear, however, if the C_L is decreased at the fixed 35-km altitude. Figure 11 shows the C_p distributions and Mach line patterns at normal (C_L = 1.26) and overspeed (C_L = 1.11) conditions at fixed reduced Mach and Reynolds numbers $\mathcal{M}$ and $\mathcal{R}$. As described earlier, this corresponds to trim changes at fixed altitude, these being typically caused by control upsets.

C. Constant-Lift Polars

Although the λ-shocks are normally undesirable, they must be tolerated to some extent if the aircraft is to quickly recover from the overspeed condition. If the airfoil suffers from massive separation, or "Mach buffet," at the overspeed condition, a large altitude loss must be incurred before the Mach number drops sufficiently to allow a pullout. Such a deficiency in the airfoil behavior is clearly unacceptable.

The C_L margin between normal operation and Mach buffet can be easily seen in a constant-lift drag polar in which the reduced parameters $\mathcal{M}$ and $\mathcal{R}$ are held fixed. Figure 12 shows five computed $\mathcal{M}$—$\mathcal{R}$ polars compared with conventional M—Re polars. Each corresponding pair was arbitrarily made to intersect at C_L = 1 by choosing $M = \mathcal{M}$ and $Re = \mathcal{R}$. The striking difference between the constant-lift and conventional polars stresses the importance of using the constant-lift $\mathcal{M}$—$\mathcal{R}$ parameterization to evaluate airfoil behavior near ceiling conditions. Mach buffet simply corresponds to the lower C_L

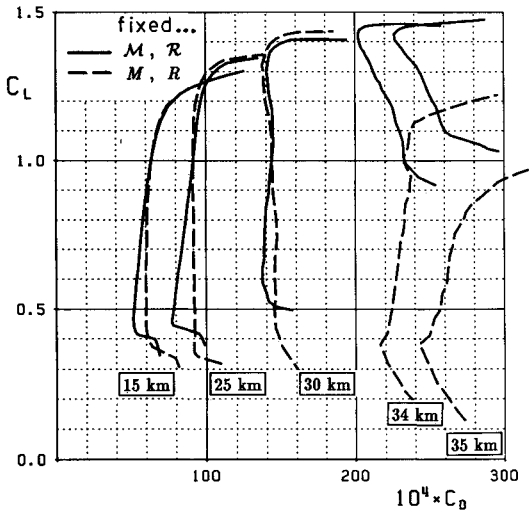

Fig. 12 Computed constant-lift $\mathcal{M}$—$\mathcal{R}$ polars compared with conventional M—Re polars for TH12 airfoil. Parameter values given in Fig. 9.

limit of the 30-, 34-, and 35-km constant-lift polars. This limit is not easily discerned in the conventional M—Re polars. Also, the constant-lift polars very clearly indicate that with the implied 200 N/m² wing loading it becomes futile to try to fly much above 35 km, as the drag-rise is rather catastrophic, and the usable C_L range shrinks to zero.

D. Lower Altitude Conditions

Airfoils designed expressly for the 35-km ceiling conditions have been found to display extremely favorable behavior at lower altitudes. The lower Mach numbers produce earlier leading-edge spikes and therefore tend to drive the maximum lift coefficients down, although the higher Reynolds numbers give quite low C_D levels. Figures 13 and 14 show the C_p distributions at 30 km and 15 km, respectively. The upper surface, which had been tailored primarily to achieve a long bubble ramp at transonic conditions, now produces a very flat upper C_p distribution ideally suited for extensive laminar flow at the higher Reynolds numbers. In fact, the airfoil appears quite competitive in L/D with modern sailplane airfoils. These results indicate that an ultrahigh altitude aircraft outfitted with the TH11-13 airfoils or something similar will not likely require trim flaps to operate efficiently over all operating altitudes.

E. Lower Surface and Airfoil Thickness

Except for the large amount of aft loading, the design of the airfoil lower surfaces is influenced primarily by structural considerations. As mentioned earlier, the TH11 and TH13 airfoils shown in Fig. 10 were designed to investigate the sensitivity to thickness. This information is necessary to allow a drag/weight tradeoff to be made for a particular vehicle.

A common difficulty which arises in combining substantial forward thickness with aft loading is that the lower boundary layer is subjected to a large adverse pressure gradient. In the present airfoil family, this can produce a very large separation bubble over most of the undercamber region at the highest altitudes. Separation bubbles on the pressure surface are in general problematic, since as C_L is increased, the pressure distribution and the chord Reynolds number both change to increase bubble losses. As pointed out by Horstmann and Quast,[6] this behavior makes the lower surface a good candidate for artificial transition, especially since the lower bubble does not move very much with C_L. In contrast, the upper surface bubble moves forward substantially as altitude and C_L is increased, significantly complicating any prospective artificial transition scheme. Also, the decrease in Reynolds number with altitude is partially compensated by the ap-

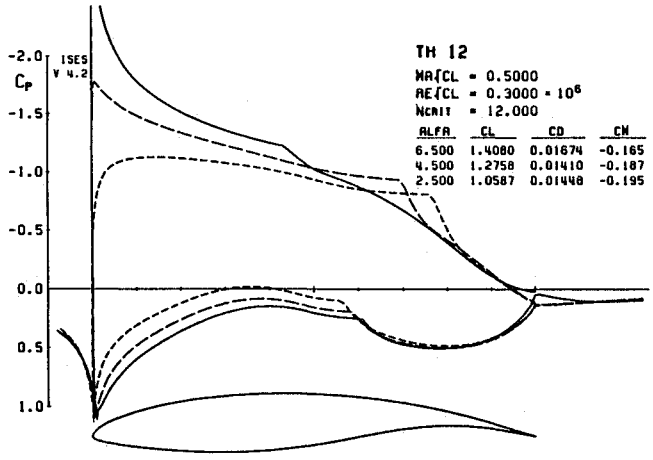

Fig. 13 C_p distributions for TH12 airfoil at 30-km operation. $\mathcal{M}$ = 0.15 and $\mathcal{R}$ = 300,000.

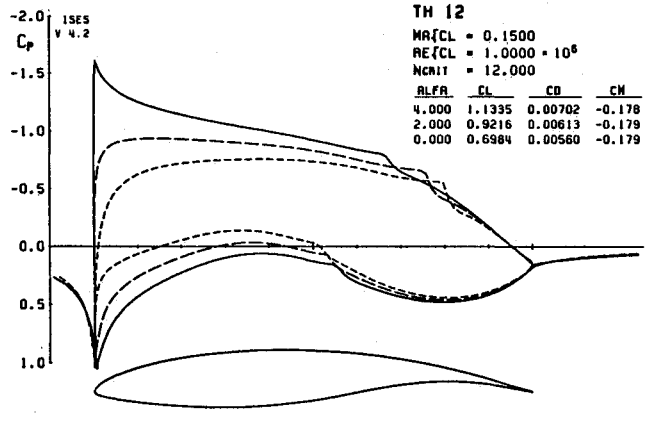

Fig. 14 C_p distributions for TH12 airfoil at 15-km operation. $\mathcal{M}$ = 0.15 and $\mathcal{R}$ = 1,000,000.

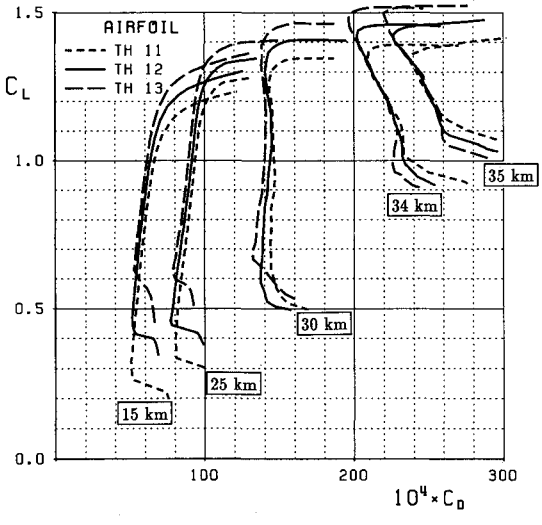

Fig. 15 Polars for TH11 (14.9%), TH12 (12.9%), and TH13 (10.9%) airfoils showing effect of airfoil thickness. $\mathcal{M}$, $\mathcal{R}$ parameters given in Fig. 9.

pearance of the instability ramp on the suction surface, which keeps bubble losses in check.

The present airfoils were designed to rely on a turbulator located near the midchord on the pressure surface. Either a pneumatic[19,6] or a mechanical turbulator could be used. The former has a lower device drag and can be modulated, and the latter has the advantage of great simplicity. In the calculations, artificial transition was simulated simply by specifying n_{crit} = 4 for the lower surface for all cases. This gives transition slightly farther aft at lower Reynolds numbers, which

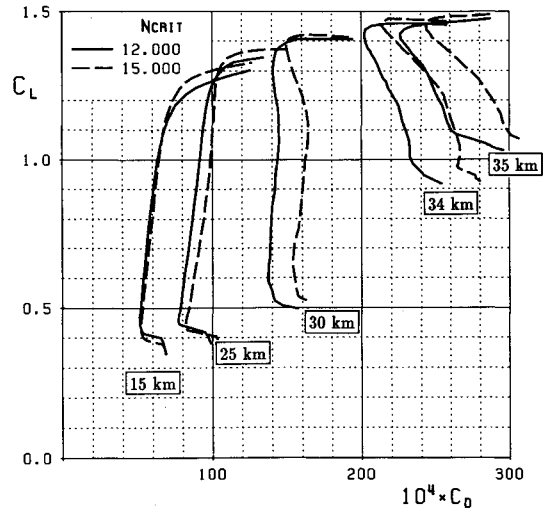

Fig. 16 Polars for TH12 airfoil showing sensitivity to the critical amplification ratio. Solid curves: n_{crit} = 12. Dashed curves: n_{crit} = 15.

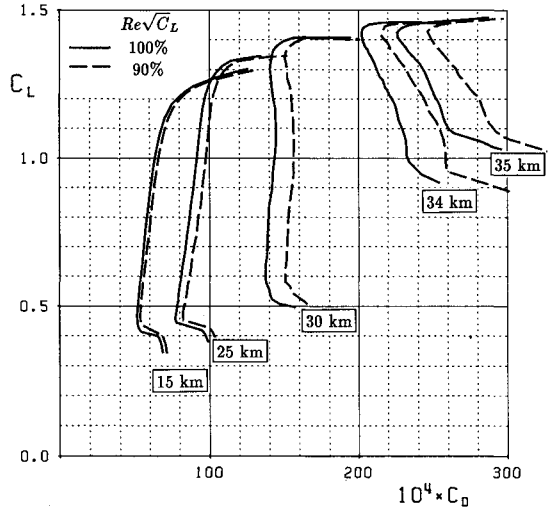

Fig. 17 Polars for TH12 airfoil showing sensitivity to the reduced Reynolds number. Solid curves: original $\mathcal{R}$. Dashed curves: $\mathcal{R}$ decreased by 10%.

mimics the increase in the gap between turbulator and transition locations as Reynolds number is lowered.

Figure 15 compares the constant-lift polars of the TH11, TH12, and TH13 airfoils. The most significant effects of increasing thickness in the present airfoil family are a reduction of maximum C_L, and a reduction in the usable C_L range at the higher altitudes. Again, a drag/weight tradeoff would have to be made for a particular vehicle in order to select the optimum thickness. Most likely a continuous decrease in thickness from wing root to tip would be used.

F. Transition Parameter Sensitivity

Given that the present transition formulation involves considerable uncertainties for flows with λ-shocks, it is prudent to investigate the sensitivity of airfoil performance to transition location. In the e^n method, this is done by varying the critical amplification ratio n_{crit}. Figure 16 compares polars for n_{crit} = 12 (used for all other calculations) and n_{crit} = 15. The lower disturbance levels implied by n_{crit} = 15 produces higher drag by delaying transition in the bubbles and increasing bubble losses. The effect is especially strong at the lowest Reynolds numbers. This suggests that a more aggressive transition ramp at ceiling conditions might be helpful in reducing drag.

G. Reduced Reynolds Number Sensitivity

At low-Reynolds numbers, optimization of wing aspect ratio must not only involve structural weight and induced drag,

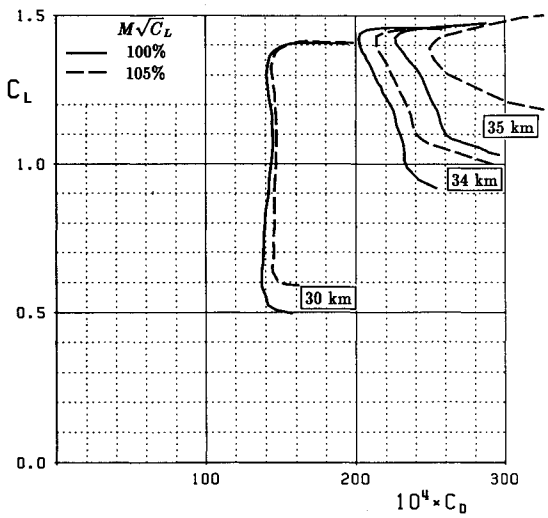

Fig. 18 Polars for TH12 airfoil showing sensitivity to the reduced Mach number. Solid curves: original $\mathcal{M}$. Dashed curves: $\mathcal{M}$ increased by 5%.

but profile drag as well. Figure 17 shows the effect of a 10% decrease in the reduced Reynolds number $\mathcal{R}$, which corresponds to an increase in the design aspect ratio from 25 to 30. As expected, the profile drag increase is greatest at low-Reynolds numbers, and is qualitatively similar to a decrease in the background disturbance level.

H. Reduced Mach Number Sensitivity

The consequence of exceeding the design wing loading (not an uncommon occurrence in practice) is primarily to increase the ceiling parameter M^2C_L, or equivalently the reduced Mach number $\mathcal{M}$ as Eq. (6) shows. An increase in gross weight also affects the reduced Reynolds number, but this contribution can be accounted for separately in a sensitivity analysis. Figure 18 shows the effect of a 5% increase in the reduced Mach number, corresponding to a 10% increase in wing loading. Only the highest altitude curves are shown, as no significant effect occurs at lower altitudes. At ceiling, the effect is quite dramatic as expected.

VI. Conclusions

The present computational study has investigated the performance and behavior of airfoils designed for operation in the transonic low-Reynolds number regime. Results indicate that 35-km altitude is attainable with the lowest practical wing loadings, but further increases in altitude produce catastrophic drag increases due to Mach and Reynolds number effects. The usefulness of examining airfoil characteristics using constant-lift polars has been demonstrated. Sensitivity studies have been performed to obtain information necessary for initial vehicle sizing and optimization.

Although the numerical analysis methodology appears to capture all the relevant flow physics for the high-Mach—low-Reynolds number regime, some uncertainties remain. To validate the method to an acceptable level of confidence, the following test data would be of great value:

1) Detailed boundary layer and surface pressure measurements of laminar shock/boundary-layer interaction flows, with significantly less three-dimensional effects and freestream turbulence than the data presently available.

2) Determination of critical amplification ratios appropriate to laminar shock/boundary-layer interactions, and a theoretical investigation of the influence of impinging λ-shocks on initial Tollmien-Schlichting wave disturbances.

3) Measurement of one or more representative airfoil drag polars in the $M \simeq 0.60$ and $Re \simeq 200{,}000$ range.

Tests of actual airfoil geometries are extremely challenging with the $M \simeq 0.60$, $Re \simeq 200{,}000$ combination. Ground-based tests would require a pressure tunnel such as the Langley low turbulence pressure tunnel pumped down to 0.1 atm or less, in order to allow the test model to have a reasonable chord. High-altitude flight tests might be an alternative approach. This may be rather costly, but can reproduce the proper freestream turbulence level—clearly an important parameter at ceiling conditions.

Acknowledgments

This research was supported by the MIT Carl Richard Soderberg Faculty Development Chair and the National Science Foundation Presidential Young Investigator Program.

References

[1]"Global Stratospheric Change: Requirements for a Very-High-Altitude Aircraft for Atmospheric Research," NASA Ames Research Center, CP 10041, 1989.

[2]McGeer, T., Langford, J. S., Anderson, J. G., and Drela, M., "Theseus: A High-Altitude Aircraft for Atmospheric Science." Aurora Flight Sciences Corp., Rept. AR 905, Alexandria, VA, Nov. 1990.

[3]Henderson, B. W., "Boeing Condor Raises UAV Performance Levels," *Aviation Week & Space Technology*, McGraw-Hill, Washington, DC, April 23, 1990, pp. 36–38.

[4]Wortmann, F. X., "Aerofoil Design for Man Powered Aircraft," *Second International Symposium on the Technology and Science of Low Speed and Motorless Flight*, MIT, Cambridge, MA, 1974.

[5]Drela, M., "Low-Reynolds Number Airfoil Design for the MIT Daedalus Prototype: A Case Study," *Journal of Aircraft*, Vol. 25, No. 8, 1988, pp. 724–732.

[6]Horstmann, K. H., and Quast, A., "Drag Reduction by Means of Pneumatic Turbulators," TR FB-81-33, DFVLR Press, Braunschweig, Germany, 1982.

[7]Pfenninger, W., and Vemuru, C. S., "Design of Low Reynolds Number Airfoils-I.," *Journal of Aircraft*, Vol. 27, No. 3, 1990, pp. 204–210.

[8]Selig, M. S., Donovan, J. F., and Fraser, D. B., *Airfoils at Low Speeds*, H. A. Stokely, Virginia Beach, VA, 1989.

[9]Giles, M. B., and Drela, M., "Two-Dimensional Transonic Aerodynamic Design Method," *AIAA Journal*, Vol. 25, No. 9, 1987, pp. 1199–1206.

[10]Drela, M., and Giles, M. B., "Viscous-Inviscid Analysis of Transonic and Low Reynolds Number Airfoils," *AIAA Journal*, Vol. 25, No. 10, 1987, pp. 1347–1355.

[11]McGhee, R. J., Walker, B. S., and Millard, B. F., "Experimental Results for the Eppler 387 Airfoils at Low Reynolds Numbers in the Langley Low-Turbulence Pressure Tunnel," NASA TM 4062, Oct. 1988.

[12]Liebeck, R. H., "Low Reynolds Number Airfoil Design for Subsonic Compressible Flow," *Conference on Low Reynolds Number Airfoil Aerodynamics*, edited by T. J. Mueller, Univ. of Notre Dame, Notre Dame, IN, June 1989, pp. 13–31.

[13]Ackeret, J., Feldmann, F., and Rott, N., "Investigations of Compression Shocks and Boundary Layers in Gases Moving at High Speed," NACA TM 1113, Jan. 1947; see also Original Rept.: Mitteilung No. 10 of the Inst. f. Aerodynamik, E.T.H. Zurich, 1946.

[14]Liepmann, H. W., "The Interaction Between Boundary Layer and Shock Waves in Transonic Flow," *Journal of the Aeronautical Sciences*, Vol. 13, No. 12, 1946, pp. 623–637.

[15]Melnik, R. E., "Turbulent Interactions on Airfoils at Transonic Speeds—Recent Developments," Conf. on Computation of Viscous-Inviscid Interactions, AGARD-CP-291, 1980.

[16]Smith, A. M. O., and Gamberoni, N., "Transition Pressure Gradient, and Stability Theory," Rept. ES 26388, Douglas Aircraft Co., 1956.

[17]van Ingen, J. L., "A Suggested Semi-Empirical Method for the Calculation of the Boundary Layer Transition Region, Rept. VTH-74, Delft Univ. of Technology, Dept. of Aerospace Engineering, The Netherlands, 1956.

[18]Mack, L. M., "Boundary-Layer Linear Stability Theory," *Special Course on Stability and Transition of Laminar Flow*, AGARD-R-709, von Karman Inst., Brussels, Belgium, June 1984, pp. 3-1–3-79.

[19]Pfenninger, W., "Untersuchungen über Reibungsverminderungen an Tragflügeln insbesondere mit Hilfe von Grenzschichtabsaugung," Inst. f. Aerodynamik E.T.H., Zürich Mitteilung, Rept. 13, Zurich, Switzerland, 1946; English translation: NACA TM 1181, 1947.